Toward a Computational Description of Nitrile Hydratase: Studies of the Ground State Bonding and Spin-Dependent Energetics of Mononuclear, Non-Heme Fe(III) Complexes

ARTICLE *in* INORGANIC CHEMISTRY · FEBRUARY 2004

Impact Factor: 4.76 · DOI: 10.1021/ic0350032 · Source: PubMed

4 AUTHORS, INCLUDING:

Christopher H Chang
National Renewable Energy Laboratory
30 PUBLICATIONS **626** CITATIONS
SEE PROFILE

Rodney J. Bartlett
University of Florida
664 PUBLICATIONS **40,698** CITATIONS
SEE PROFILE

Inorg. Chem. **2004**, *43*, 458–472

Toward a Computational Description of Nitrile Hydratase: Studies of the Ground State Bonding and Spin-Dependent Energetics of Mononuclear, Non-Heme Fe(III) Complexes

Christopher H. Chang,[†] Amy J. Boone,[‡] Rodney J. Bartlett, and Nigel G. J. Richards*

Department of Chemistry, University of Florida, Gainesville, Florida 32611-7200

Received August 25, 2003

The metal coordination and spin state of the Fe(III) center in nitrile hydratase (NHase) has stimulated the synthesis of model complexes in efforts to understand the reactivity and spectroscopic properties of the enzyme. We report density functional theory (DFT) calculations on a number of Fe(III) complexes that have been prepared as models of the NHase metal center, together with others having similar ligands but different ground state spin multiplicities. Our results suggest that a DFT description of specific spin configurations in these systems does not suffer from significant amounts of spin contamination. In particular, B3LYP calculations not only reproduce the observed spin state preferences of these Fe(III) complexes but also predict spin-dependent structural properties consistent with those expected on the basis of ligand field models. An analysis of the natural bond orbital (NBO) transformation of the Kohn–Sham wave functions has enabled quantitation of the overall contribution to covalency of ligand-to-metal σ-donation and π-donation, and metal-to-ligand π-back-bonding in these Fe(III) complexes at their BLYP-optimized geometries. Although sulfur ligands are the primary source of covalency in the Fe(III) complexes, our quantitative analysis suggests that hyperbonding between metal-bound nitrogens and an Fe–S bond represents a mechanism by which Fe–N covalency may arise. These studies establish the computational methodology for future theoretical investigations of the NHase Fe(III) center.

Introduction

The metal coordination and spin state of the Fe(III) center in nitrile hydratase (NHase)[1−3] has stimulated the synthesis of numerous model complexes in efforts to understand the reactivity and spectroscopy of the enzyme.[4] In principle, theoretical calculations might also provide insight into the electronic properties of the NHase metal center, but accurately determining relative energies for the many energetically low-lying spin states accessible to open-shell Fe(III) complexes is a computational challenge.[5] Hartree−Fock approaches are not suitable for computing the properties of these compounds because electron correlation must be taken into account. Although post-Hartree−Fock ab initio methods for including electron correlation such as MCSCF[6] and CASPT2[7] are available, in practice these are generally limited to only a few configurations or active orbitals, precluding their routine use for geometry optimization and single-point

* Corresponding author. E-mail: richards@qtp.ufl.edu.

[†] Recipient of an NIH postdoctoral fellowship (DK61193).

[‡] Present address: Department of Biochemistry and Biophysics, University of North Carolina, Chapel Hill, NC 27599.

(1) (a) Tsujimura, M.; Dohmae, N.; Odaka, M.; Chijimatsu, M.; Takio, K.; Yohda, M.; Hoshino, M.; Nagashima, S.; Endo, I. *J. Biol. Chem.* **1997**, *272*, 29454−29459. (b) Huang, W.; Jia, J.; Cummings, J.; Nelson, M.; Schneider, G.; Lindqvist, Y. *Structure* **1997**, *5*, 691−699. (c) Nagashima, S.; Nakasako, M.; Dohmae, N.; Tsujimura, M.; Takio, K.; Odaka, M.; Yohda, M.; Kamiya, N.; Endo, I. *Nat. Struct. Biol.* **1998**, *5*, 347−351. (d) Nakasako, M.; Odaka, M.; Yohda, M.; Dohmae, N.; Takio, K.; Kamiya, N.; Endo, I. *Biochemistry* **1999**, *38*, 9887−9898.

(2) Sugiura, Y.; Kuwahara, J.; Nagasawa, T.; Yamada, H. *J. Am. Chem. Soc.* **1987**, *109*, 5848−5850.

(3) (a) Endo, I.; Nojiri, M.; Tsujimura, M.; Nakasako, M.; Nagashima, S.; Yohda, M.; Odaka, M. *J. Inorg. Biochem.* **2001**, *83*, 247−253. (b) Kobayashi, M.; Shimizu, S. *Curr. Opin. Chem. Biol.* **2000**, *4*, 95−102. (c) Endo, I.; Odaka, M.; Yohda, M. *Trends Biotechnol.* **1999**, *17*, 244−249.

(4) (a) Mascharak, P. K. *Coord. Chem. Rev.* **2002**, *225*, 201−214. (b) Marlin, D. S.; Mascharak, P. K. *Chem. Soc. Rev.* **2000**, *29*, 69−74. (c) Artaud, I.; Chatel, S.; Chauvin, A. S.; Bonnet, D.; Kopf, M. A.; Leduc, P. *Coord. Chem. Rev.* **1999**, *190−192*, 577−586.

(5) (a) Ghosh, A.; Taylor, P. R. *Curr. Opin. Chem. Biol.* **2003**, *7*, 113−124. (b) Harvey, J. N.; Poli, R.; Smith, K. M. *Coord. Chem. Rev.* **2003**, *238−239*, 347−361. (c) Salahub, D. R.; Zerner, M. C. In *The Challenge of d and f Electrons*; Salahub, D. R., Zerner, M. C., Eds.; ACS Symposium Series 394; American Chemical Society: Washington, DC, 1989; pp 1−16.

(6) (a) Gilson, H. S. R.; Krauss, M. *J. Phys. Chem. A* **1998**, *102*, 6525−6532. (b) Schmidt, M. W.; Gordon, M. S. *Annu. Rev. Phys. Chem.* **1998**, *49*, 233−266.

10.1021/ic0350032 CCC: $27.50
Published on Web 12/13/2003

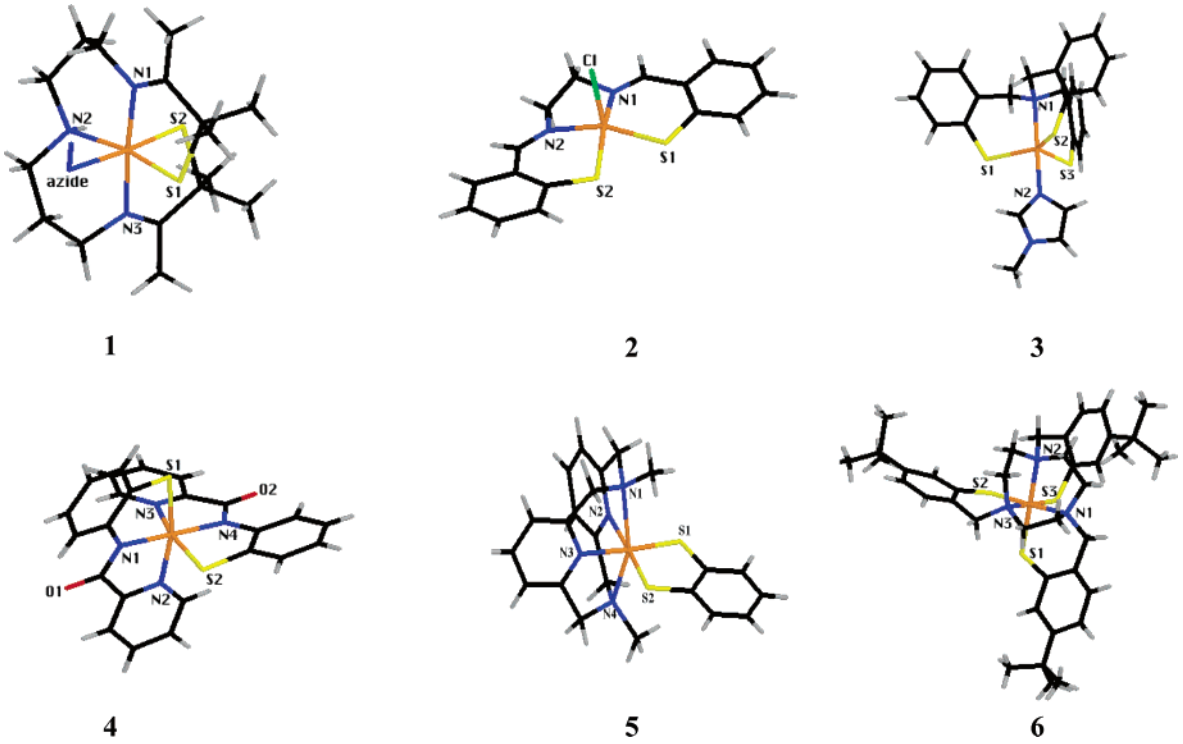

Figure 1. X-ray crystal structures of ferric complexes **1**−**6**: **1**, azido(2,3,13,14-tetramethyl-4,8,12-triaza-3,12-pentadecadiene-2,14-dimercapto)iron(III);[23] **2**, chloro(*N*,*N*′-ethylenebis(mercaptosalicylidene-iminato)iron(III);[24] **3**, (1-methylimidazolyl)[tris(2-mercaptobenzyl)amino]iron(III);[25] **4**, bis(*N*-2-mercaptophenyl-2′-pyridinocarboxamidato)iron(III);[26] **5**, (1,2-benzenedimercapto)[*N*,*N*′-dimethyl-2,11-diaza[3.3]-(2,6)-pyridinophane]iron(III);[27] **6**, [1,4,7-tris(4-*tert*-butyl-2-mercaptobenzyl)-1,4,7-triaza-cyclononane]iron(III).[28] Atoms are colored using the following scheme: C, black; H, white; N, blue; O, red; S, yellow; Fe, orange; Cl, green.

energy calculations upon biochemically interesting Fe-containing structures.[8] The technical problems are exacerbated by spin contamination in the calculated molecular wave functions, particularly when the transition metal has a low spin electronic configuration.[9] While density functional theory (DFT) methods have been shown to reproduce the structural properties of several biologically interesting transition metal centers,[10] their application to defining the ground state spin multiplicities of Fe-containing systems has been the focus of relatively few systematic investigations.[11] Indeed, the validity of using DFT calculations to sort metal spin states has been questioned because DFT is considered to model ground rather than electronic excited states.[12] Nevertheless, it has been established that the lowest energy state of systems in a particular spatial and spin symmetry is formally accessible via DFT,[13] even though the transferability of current functionals to describe excited state densities remains to be definitively demonstrated.

As part of our ongoing efforts[14] to understand the electronic properties of the mononuclear, non-heme metal center in Fe-dependent NHase,[1,3] we now report a series of DFT calculations on Fe(III) complexes that have been specifically prepared as models of the metal center in the enzyme (Figure 1). A number of Fe(III) complexes possessing similar N/S ligands but different coordination geometries have also been studied so as to explore the general utility of this computational approach. Our results suggest that a DFT description of specific spin configurations in these systems does not suffer from significant amounts of spin contamination, and lay a firm foundation for employing future BLYP and B3LYP calculations to determine the structural basis and mechanistic importance of the unique spin properties observed for the Fe(III) center in NHase.[3] Natural bond orbital

(7) (a) Pierloot, K.; De Kerpel, J. O. A.; Ryde, U.; Roos, B. O. *J. Am. Chem. Soc*. **1997**, *119*, 218−226. (b) Roos, B. O.; Andersson, K.; Fülscher, M. P.; Malmqvist, P.-Å.; Serrano-Andrés, L.; Pierloot, K.; Merchan, M. *Adv. Chem. Phys*. **1996**, *93*, 219−331.
(8) (a) Lovell, T.; Himo, F.; Han, W.-G.; Noodleman, L. *Coord. Chem. Rev*. **2003**, *238*−*239*, 211−232. (b) Friesner, R. A.; Baik, M.-H.; Gherman, B. F.; Guallar, V.; Wirstam, M.; Murphy, R. B.; Lippard, S. J. *Coord. Chem. Rev*. **2003**, *238*−*239*, 267−290. (c) Siegbahn, P. E. M. *J. Comput. Chem*. **2001**, *22*, 1634−1645. (d) Siegbahn, P. E. M.; Blomberg, M. R. A. *Chem. Rev*. **2000**, *100*, 421−437. (e) Niu, S.; Hall, M. B. *Chem. Rev*. **2000**, *100*, 353−405. (f) Siegbahn, P. E. M. *Adv. Chem. Phys*. **1996**, *93*, 333−387.
(9) Schlegel, H. B. *Encyclopedia of Computational Chemistry*; Schleyer, P. v. R., Allinger, N. L., Clark, T., Gasteiger, J., Kollman, P. A., Schaefer, H. F., III, Schreiner, P. R., Eds.; Wiley: Chichester, 1998; pp 2665−2671.
(10) (a) Siegbahn, P. E. M. *Curr. Opin. Chem. Biol*. **2002**, *6*, 227−235. (b) Ghosh, A.; Steene, E. *J. Biol. Inorg. Chem*. **2001**, *6*, 739−752. (c) Harris, D. L. *Curr. Opin. Chem. Biol*. **2001**, *5*, 724−735. (d) Spiro, T. G.; Zgierski, M. Z.; Kozlowski, P. M. *Coord. Chem. Rev*. **2001**, *219*−*221*, 923−936. (e) Li, S.; Hall, M. B. *Inorg. Chem*. **2001**, *40*, 18−24. (f) Siegbahn, P. E. M.; Blomberg, M. R. A. *Annu. Rev. Phys. Chem*. **1999**, *50*, 221−249. (g) Friesner, R. A.; Beachy, M. D. *Curr. Opin. Struct. Biol*. **1998**, *8*, 257−262.
(11) (a) Staroverov, V. N.; Davidson, E. R. *Chem. Phys. Lett*. **2001**, *340*, 142−150. (b) Kozlowski, P. M.; Spiro, T. G.; Bérces, A.; Zgierski, M. Z. *J. Phys. Chem. B* **1998**, *102*, 2603−2608. (c) Harris, D.; Loew, G. H.; Komornicki, A. *J. Phys. Chem. A* **1997**, *101*, 3959−3965.
(12) Stückl, A. C.; Daul, C. A.; Güdel, H. U. *Int. J. Quantum Chem*. **1997**, *61*, 579−588.
(13) (a) Gunnarsson, O.; Lundqvist, B. I. *Phys. Rev. B* **1976**, *13*, 4274−4298. (b) von Barth, U. *Phys. Rev. A* **1979**, *20*, 1693−1703.
(14) (a) Greene, S. N.; Chang, C. H.; Richards, N. G. J. *Chem. Commun*. **2002**, 2386-2387. (b) Boone, A. J.; Chang, C. H.; Greene, S. N.; Herz, T.; Richards, N. G. J. *Coord. Chem. Rev*. **2003**, *238*−*239*, 291−314.

(NBO) analyses[15] of the optimized ground state structures of the six complexes, together with consideration of delocalization effects and three-centered bonding involving Fe, have also identified metal−ligand interactions that may be important in conferring a low spin ground state on the mononuclear, non-heme Fe(III) center of the enzyme.

Computational Methodology

The TURBOMOLE software package[16] was used to perform all DFT calculations employing the BLYP exchange-correlation functional,[17,18] and to compute a small number of single-point B3LYP energies, which are explicitly specified in the text. All other single point energies were calculated using the B3LYP functional[19,20] as implemented in *Gaussian98*.[21] We note that the *Gaussian98* implementation of B3LYP differs from that coded in TURBOMOLE. More specifically, the third form of the VWN local correlation functional (VWN-III) is used in *Gaussian98*, while TURBOMOLE employs the fifth form (VWN-V).[22]

The atomic coordinates for the Fe(III) complexes **1**−**6** (Figure 1)[23−28] were obtained from either the Cambridge Crystallographic Database,[29] release 5.14 (**2**, **3**, **5**, and **6**), or from coordinate data supplied as Supporting Information in relevant publications (**1** and **4**).[23,26] For all complexes except **2**, hydrogen atom positions were obtained from crystallographic coordinates. In the case of complex **2**, appropriate hydrogens were added to heavy atoms in standard geometries using CACHe WorkSystem Pro 5.0 (CACHe Group, Fujitsu America Inc., Beaverton, OR). Structural superimpositions were performed using the MOLDEN package (version 3.6),[30] or the CACHe software in the case of complex **6**.

Separate single-point energies were computed for the doublet, quartet, and sextet spin configurations of each of these six Fe(III) complexes at their experimental geometries, using both the BLYP and B3LYP density functionals. Bond lengths and angles in these initial structures differed very slightly from those seen in the crystal structures as a consequence of converting fractional crystal coordinates into a format suitable for subsequent use in TURBOMOLE and/or *Gaussian98*. A careful comparison of the differences, however, revealed that these changes were within the estimated error of the experimental measurements (Table S1, Supporting Information) and are therefore unlikely to have any significant impact on the results of our DFT studies. All calculations employed a 6-31G* basis, although polarization functions were not included on carbon atoms.[31] Except where noted in the tables and text, the density matrix in all single point energy determinations was converged to a tight RMS threshold of 1.0×10^{-8}. SCF convergence problems could generally be avoided by first performing a Hartree−Fock calculation with either a STO-3G or 3-21G* basis set from the automatically generated initial guess, with the resulting orbitals used as input for subsequent DFT calculations. To achieve convergence in more difficult cases, we also employed a strategy in which the initial Hartree−Fock SCF was converged for either the closed-shell electronic configuration (cation) or the system containing two fewer electrons. In calculations of the vertical transition energies of Fe(III) complexes **3** and **6** at their experimental geometries, an SCF convergence criterion of 10^{-8} E_h in the SCF energy was used rather than the RMS change in the density matrix. Due to problems obtaining SCF convergence, relative energies and $\langle S^2 \rangle_{KS}$ values evaluated from the Kohn−Sham reference determinant for **3** and **6** were computed using TURBOMOLE instead of *Gaussian98*. Although the B3LYP energies calculated for a given spin state using *Gaussian98* and TURBOMOLE have different absolute values, relative spin state energies from either software package generally differ by an inconsequential amount (less than 1 kcal/mol).

The geometries of complexes **1**−**3** were optimized at each of their three possible spin states using the BLYP functional, as were the geometries of **4**−**6** at their observed spin multiplicities. In the case of complex **5**, the initial structure was that observed at 295 K. These geometry optimizations were converged to a gradient of no more than 10^{-3} E_h/Bohr, using an SCF convergence criterion of 10^{-6} E_h/cycle. For the largest Fe(III) complex, **6**, fast Coulomb approximation methods,[32] as implemented in TURBOMOLE, were used in a preliminary geometry optimization starting from the experimental coordinates. The minimized structure was then optimized further without Coulomb fitting, allowing the calculation to converge within a few cycles. Since the initial Coulomb fitting procedure requires an auxiliary basis set matched to the standard

(15) (a) Reed, A. E.; Curtiss, L. A.; Weinhold, F. *Chem. Rev.* **1988**, *88*, 899−926. (b) Weinhold, F. In *Encyclopedia of Computational Chemistry*; Schleyer, P. v. R., Allinger, N. L., Clark, T., Gasteiger, J., Kollman, P. A., Schaefer, H. F., III, Schreiner, P. R., Eds.; Wiley: Chichester, 1998; pp 1792−1811.

(16) (a) Von Arnim, M.; Ahlrichs, R. *J. Comput. Chem.* **1998**, *19*, 1746−1757. (b) Ahlrichs, R.; Bär, M.; Häser, M.; Horn, H.; Kölmel, C. *Chem. Phys. Lett.* **1989**, *162*, 165−169.

(17) Becke, A. D. *Phys. Rev. A* **1988**, *38*, 3098−3100.

(18) Lee, C.; Yang, W.; Parr, R. G. *Phys. Rev. B* **1988**, *37*, 785−789.

(19) Becke, A. D. *J. Chem. Phys.* **1993**, *98*, 5648−5652.

(20) Stephens, P. J.; Devlin, F. J.; Chabalowski, C. F.; Frisch, M. J. *J. Phys. Chem.* **1994**, *98*, 11623−11627.

(21) Frisch, M. J.; Trucks, G. W.; Schlegel, H. B.; Scuseria, G. E.; Robb, M. A.; Cheeseman, J. R.; Zakrzewski, V. G.; Montgomery, J. A., Jr.; Stratmann, R. E.; Burant, J. C.; Dapprich, S.; Millam, J. M.; Daniels, A. D.; Kudin, K. N.; Strain, M. C.; Farkas, O.; Tomasi, J.; Barone, V.; Cossi, M.; Cammi, R.; Mennucci, B.; Pomelli, C.; Adamo, C.; Clifford, S.; Ochterski, J.; Petersson, G. A.; Ayala, P. Y.; Cui, Q.; Morokuma, K.; Malick, D. K.; Rabuck, A. D.; Raghavachari, K.; Foresman, J. B.; Cioslowski, J.; Ortiz, J. V.; Stefanov, B. B.; Liu, G.; Liashenko, A.; Piskorz, P.; Komaromi, I.; Gomperts, R.; Martin, R. L.; Fox, D. J.; Keith, T.; Al-Laham, M. A.; Peng, C. Y.; Nanayakkara, A.; Gonzalez, C.; Challacombe, M.; Gill, P. M. W.; Johnson, B. G.; Chen, W.; Wong, M. W.; Andres, J. L.; Head-Gordon, M.; Replogle, E. S.; Pople, J. A. *Gaussian 98*, revision A.7; Gaussian, Inc.: Pittsburgh, PA, 1998.

(22) Vosko, S. H.; Wilk, L.; Nusair, M. *Can. J. Phys.* **1980**, *58*, 1200−1211.

(23) Ellison, J. J.; Nienstedt, A.; Shoner, S. C.; Barnhart, D.; Cowen, J. A.; Kovacs, J. A. *J. Am. Chem. Soc.* **1998**, *120*, 5691−5700.

(24) Fallon, G. D.; Gatehouse, B. M.; Marini, P. J.; Murray, K. S.; West, B. O. *J. Chem. Soc., Dalton Trans.* **1984**, 2733−2739.

(25) Govindaswamy, N.; Quarless, D. A., Jr.; Koch, S. A. *J. Am. Chem. Soc.* **1995**, *117*, 8468−8469.

(26) Noveron, J. C.; Olmstead, M. M.; Mascharak, P. K. *Inorg. Chem.* **1998**, *37*, 1138−1139.

(27) Koch, W. O.; Schünemann, V.; Gerdan, M.; Trautwein, A. X.; Krüger, H.-J. *Chem. Eur. J.* **1998**, *4*, 686−691.

(28) Beissel, T.; Bürger, K. S.; Voigt, G.; Wieghardt, K.; Butzlaff, C.; Trautwein, A. X. *Inorg. Chem.* **1993**, *32*, 124−126.

(29) Allen, F. H.; Bellard, S.; Brice, M. D.; Cartwright, B. A.; Doubleday: A.; Higgs, H.; Hummelink, T.; Hummelink-Peters, B. G.; Kennard, O.; Motherwell, W. D. S.; Rodgers, J. R.; Watson, D. G. *Acta Crystallogr., Sect. B* **1979**, *35*, 2331−2339.

(30) Schaftenaar, G.; Noordik, J. H. *J. Comput.-Aided Mol. Des.* **2000**, *14*, 123−134. This software package can be obtained from http://www.cmbi.kun.nl/~schaft/molden/molden.html.

(31) (a) Hehre, W. J.; Ditchfield, R.; Pople, J. A. *J. Chem. Phys.* **1972**, *56*, 2257−2261. (b) Hariharan, P. C.; Pople, J. A. *Theor. Chim. Acta* **1973**, *28*, 213−222. (c) Francl, M. M.; Pietro, W. J.; Hehre, W. J.; Binkley, J. S.; Gordon, M. S.; DeFrees, D. J.; Pople, J. A. *J. Chem. Phys.* **1982**, *77*, 3654−3665. (d) Rassolov, V.; Pople, J. A.; Ratner, M. A.; Windus, T. L. *J. Chem. Phys.* **1998**, *109*, 1223−1229. (e) Feller, D.; Davidson, E. R. In *Reviews in Computational Chemistry, Vol. 1*; Lipkowitz, K. B., Boyd, D. B., Eds.; VCH: New York, 1990; pp 1−43.

(32) (a) Eichkorn, K.; Treutler, O.; Öhm, H.; Häser, M.; Ahlrichs, R. *Chem. Phys. Lett.* **1995**, *240*, 283−290. (b) Eichkorn, K.; Weigend, F.; Treutler, O.; Ahlrichs, R. *Theor. Chem. Acc.* **1997**, *97*, 119−124.

one, the double-ζ plus polarization SVP basis[33] was used for geometry optimization of **6**. The wave function stability for the optimized structures of **1**−**6** at their observed spin multiplicity was verified by time-dependent BLYP calculations (data not shown).[34] Relative energies were not corrected for zero-point contributions because previous studies on $Fe(H_2O)_6^{3+}$ suggest that such corrections make no difference in the relative ordering of different spin configurations.[11c]

The converged BLYP molecular orbital coefficients were employed as initial guesses for all B3LYP computations on complexes **1**−**5**. Using the density matrices obtained from B3LYP single point calculations, NBO analyses[15] were performed for Fe(III) complexes **1**−**5** at their optimized ground state geometries by processing *Gaussian98*-generated NBO archive files with the standalone NBO 5.0 package.[35] The large number of atoms in Fe(III) complex **6** mandated the use of an alternative procedure for performing the NBO analysis. A B3LYP/LACVP* single-point calculation on **6** at its BLYP-optimized geometry was performed with Jaguar 5.0 (Schrodinger LLC, Portland, OR), subsequent analysis being carried out using NBO 5.0 as for complexes **1**−**5**. This single-point calculation was converged to 10^{-7} RMS change in the density matrix, and 10^{-6} E_h in energy/cycle, from an initial guess based on ligand field theory.[36] Initial Fe valencies from +3 to 0 were tested; the configuration corresponding to Fe^{+1} bound to two neutral sulfur atoms was found to converge to the lowest energy, probably reflecting the significant polarizability of the thiolate ligands. We note that the LACVP* basis[37] is identical to 6-31G* except for the effective core potential used on the Fe atom, and hence, the NBO analysis should be qualitatively comparable for all six complexes.

Results and Discussion

We investigated the likely utility of DFT calculations in studies of the Fe(III) center in NHase by calculating the properties of a series of six Fe(III) complexes that possess mixed sulfur and nitrogen ligands (Figure 1).[23−28] X-ray crystallographic structures are available for all of these complexes, three of which (**1**, **4**, and **6**) have been prepared specifically as models for the NHase metal center. In addition, our test set was chosen to encompass a variety of charge states, ground spin states, and coordination geometries (Table 1), thereby improving our chances of identifying any unexpected systematic biases in our DFT calculations. Experimental measurements show complexes **1**, **4**, and **6** to have a doublet ground state, while **2** and **3** adopt quartet and sextet spin states, respectively. The remaining Fe(III) complex **5** exhibits temperature-dependent spin-crossover in the range 0−300 K, and separate single-point calculations on this compound were performed on the experimental structures determined at 153 and 295 K.[27] Superimposition of the structures of **5** observed at the two temperatures clearly shows the relatively small structural differences that may impact the spin state energetics of this Fe(III) complex (Figure 2). Counterions and solvent molecules observed in the crystal were not included in these calculations, however, leaving solvation effects as a potential systematic perturbation outside the scope of this work.

Table 1. Selected Molecular Properties of Fe(III) Complexes **1**−**6**

complex	coordination geometry	net charge[a]	obsd spin state	ref
1	octahedral	0	1/2	23
2	square pyramidal	0	3/2	24
3	trigonal bipyramidal	0	5/2	25
4	octahedral	−1	1/2	26
5	octahedral	+1	3/2[b]	27
6	octahedral	0	1/2	28

[a] Counterions are not included in these calculations. [b] This molecule exhibits temperature-dependent spin-crossover. The experimentally determined spin multiplicity given in this entry corresponds to that observed for the complex at 295 K.

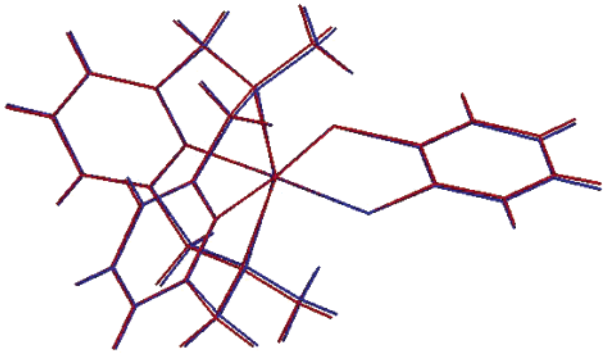

Figure 2. Superimposed high and low temperature crystal structures of Fe(III) complex **5**. Structures are colored using the following scheme: 153 K, blue; 295 K, red.

DFT Calculations of Vertical Transition Energies. The relative energies of the lowest energy doublet, quartet, and sextet states were calculated for complexes **1**−**6** at their observed geometries using the B3LYP and BLYP functionals (Table 2). In the case of complexes **1**−**4** and **6**, DFT calculations employing the B3LYP functional predicted ground state spin multiplicities that were in agreement with experimental observations. While this was also true for calculations on complexes **1**, **2**, **4**, and **6** using the BLYP functional, a doublet ground state was predicted for complex **3** rather than the sextet that is observed for this molecular geometry. It is difficult to interpret this result in light of the small energy differences that were calculated using BLYP for each of the spin states of **3**. The noticeable deviation of $\langle S^2 \rangle_{KS}$ from its theoretical value suggests that the energy for the BLYP doublet is too low because of spin contamination, in which case a modified approximation might reproduce the correct ground state, if not the ordering of excited states. The validity and limitations of employing the value of $\langle S^2 \rangle_{KS}$, as computed from a single determinant of Kohn−Sham orbitals, has been discussed elsewhere.[14b] These data also confirm that the BLYP functional tends to stabilize low spin configurations of these Fe(III) complexes to a greater extent than B3LYP, as previously reported.[38] Given that the BLYP functional reproduced the ground state spin multiplicities of

(33) Schäfer, A.; Horn, H.; Ahlrichs, R. *J. Chem. Phys.* **1992**, *97*, 2571−2577. Basis sets used in this study can be downloaded from ftp://ftp.chemie.uni-karlsruhe.de/pub.
(34) Bauernschmitt, R.; Ahlrichs, R. *Chem. Phys. Lett.* **1996**, *256*, 454−464.
(35) Glendening, E. D.; Badenhoop, J. K.; Reed, A. E.; Carpenter, J. E.; Bohmann, J. A.; Morales, C. M.; Weinhold, F. *NBO 5.0*; Theoretical Chemistry Institute, University of Wisconsin: Madison, WI, 2001.
(36) Vacek, G.; Perry, J. K.; Langlois, J.-M. *Chem. Phys. Lett.* **1999**, *310*, 189−194.
(37) Hay, P. J.; Wadt, W. R. *J. Chem. Phys.* **1985**, *82*, 299−310.

Table 2. Relative Spin State Energies and Noninteracting $\langle S^2\rangle_{KS}$ Values Calculated Using DFT Methods or the PUHF-INDO/S Semiempirical Model for Fe(III) Complexes **1**−**6** at Their Experimental Geometries[a]

	BLYP/6-31G*			B3LYP/6-31G*			PUHF-INDO/S
complex	energy (cm^{-1})	$<S^2>_{KS}$[b]	$2S+1$	energy (cm^{-1})	$\langle S^2\rangle_{KS}$[b]	$2S+1$	energy (cm^{-1})[c]
				1 (Doublet)			
$M_S = 1/2$	0	0.76	2.01	0	0.77	2.01	0
$M_S = 3/2$	9465	3.80	4.03	7515	3.82	4.04	3228
$M_S = 5/2$	17148	8.76	6.00	10202	8.76	6.00	4673
				2 (Quartet)			
$M_S = 1/2$	1864	1.20	2.41	4418	1.48	2.63	9636
$M_S = 3/2$	0	3.79	4.02	0	3.82	4.03	0
$M_S = 5/2$	9022	8.76	6.00	6049	8.76	6.00	6735
				3 (Sextet)			
$M_S = 1/2$	*0*	0.96	2.20	5870	1.18	2.39	9265
$M_S = 3/2$	*86*	3.82	4.03	3040	3.89	4.07	1779
$M_S = 5/2$	*642*	8.76	6.00	0	8.76	6.00	0
				4 (Doublet)			
$M_S = 1/2$	0	0.77	2.02	0	0.78	2.03	0
$M_S = 3/2$	10561	3.81	4.03	8040	3.81	4.03	9013
$M_S = 5/2$	18828	8.77	6.00	11563	8.77	6.01	11571
				5 (Doublet; 153 K)			
$M_S = 1/2$	0	0.77	2.02	*808*	0.83	2.07	*1919*
$M_S = 3/2$	2255	3.82	4.03	0	3.84	4.04	0
$M_S = 5/2$	13084	8.76	6.00	*6384*	8.76	6.00	*8417*
				5 (Quartet; 295 K)			
$M_S = 1/2$	470	0.98	2.22	3296	1.20	2.41	4713
$M_S = 3/2$	0	3.82	4.03	0	3.85	4.05	0
$M_S = 5/2$	9994	8.76	6.00	5686	8.76	6.00	8121
				6 (Doublet)			
$M_S = 1/2$	0	0.77	2.02	0	0.80	2.05	0
$M_S = 3/2$	6404	3.79	4.02	4018	3.84	4.04	4197
$M_S = 5/2$	9222	8.76	6.00	4114	8.76	6.00	6091

[a] Results from calculations that identify the incorrect ground spin multiplicity are italicized. [b] $2S+1 = (4\langle S^2\rangle_{KS}+1)^{1/2}$. [c] PUHF−INDO/S energies are taken from ref 41 and are included for ease of comparison.

complexes **1**, **2**, **4**, and **6**, it is likely that BLYP calculations will identify the proper ground state spin for compounds in which the ΔSCF vertical transition energies are large, even if there is some degree of spin contamination present in the wave function.

These studies also offered an opportunity to calibrate the performance of projected unrestricted Hartree−Fock (PUHF) calculations,[39] using the intermediate neglect of differential overlap (INDO/S) semiempirical Hamiltonian,[40] that were employed in our previous study of the spin preferences and spin-dependent properties of Fe(III) complexes.[41] Despite the widespread use of the PUHF-INDO/S method to compute spin multiplicities,[42] the comparison herein appears to be the first example of such an analysis. In general, PUHF-INDO/S calculations ordered the spin states identically to B3LYP, with the exception of complex **2**, for which the doublet and sextet state orders were reversed (Table 2). The energies of the $M_S = 1/2$ states in the BLYP calculations appear to be systematically stabilized relative to those obtained in PUHF-INDO/S calculations. This difference may be a consequence of a lack of orbital-dependent exchange in the BLYP functional. Since Hartree−Fock exchange tends to stabilize higher spin multiplicities, one might expect that the PUHF method would yield higher energy doublet configurations than BLYP, at least in relative terms.

PUHF−INDO/S calculations predict a different ordering of the higher spin states of complex **2** when compared with BLYP and B3LYP, an observation that deserves further consideration in light of the successes of the PUHF method.[42] It is possible that the disagreement between the DFT and PUHF-INDO/S calculations for Fe(III) complex **2** might arise from an artifactual lowering of the energy computed for the doublet spin state due to spin contamination of the Kohn−Sham wave function, reversing the spin state ordering predicted by the DFT calculations. This hypothesis is supported by the observed $\langle S^2\rangle_{KS}$ value for the doublet state of **2** when computed using the B3LYP functional (Table 2). Thus, although all methods correctly predict the experimental ground state spin multiplicity, the order of excited states in this complex remains unclear.

The availability of high and low temperature structures for complex **5**, which bracket a temperature-dependent spin transition,[27] provided an opportunity to evaluate the sensitivity of calculated spin state energies to small changes in molecular structure. Both semiempirical and DFT methods predict correctly that **5** is a ground state quartet at the structure of the Fe(III) complex determined at 295 K. When these single-point calculations were repeated using the low temperature (153 K) structure, only the BLYP functional predicted a ground state doublet in agreement with experiment. As noted elsewhere,[38] this may merely reflect the tendency of BLYP to stabilize low spin configurations of these Fe(III) complexes to a greater extent than B3LYP. Even though B3LYP calculations did not correctly predict the doublet ground state of **5** for the low temperature structure, the energy separation computed for the doublet and quartet states is only 808 cm^{-1} (2.3 kcal/mol) (Table 2). This value lies within the demonstrated uncertainty of the B3LYP model,[8f] and the small energetic separation calculated for these states is consistent with the spin crossover behavior reported for this complex.[27] Notably, the B3LYP vertical transition energies calculated for the other five compounds are all greater than 3000 cm^{-1} (8.5 kcal/mol). The PUHF-INDO/S model also fails to predict the lowest energy spin state for complex **5** at its low temperature structure.

(38) (a) Reiher, M.; Salomon, O.; Hess, B. A. *Theor. Chem. Acc.* **2001**, *107*, 48−55. (b) Salomon, O.; Reiher, M.; Hess, B. A. *J. Chem. Phys.* **2002**, *117*, 4729−4737.

(39) (a) Cory, M. G.; Zerner, M. *J. Phys. Chem. A* **1999**, *103*, 7287−7293. (b) Cory, M. G.; Stavrev, K. K.; Zerner, M. C. *Int. J. Quantum Chem.* **1997**, *63*, 781−795. (c) Harriman, J. E. *J. Chem. Phys.* **1964**, *40*, 2827−2839. (d) Sasaki, F.; Ohno, K. *J. Math. Phys.* **1963**, *4*, 1140−1147. (e) Phillips, D. H.; Schug, J. C. *J. Chem. Phys.* **1974**, *61*, 1031−1039. (f) Hardisson, A.; Harriman, J. E. *J. Chem. Phys.* **1967**, *46*, 3639−3648. (g) Sando, K. M.; Harriman, J. E. *J. Chem. Phys.* **1967**, *47*, 180−185.

(40) (a) Zerner, M. C.; Loew, G. H.; Kirchner, R. F.; Mueller-Westerhoff, U. T. *J. Am. Chem. Soc.* **1980**, *102*, 589−599. (b) Zerner, M. C. In *Reviews in Computational Chemistry, Vol. 2*; Lipkowitz, K. B., Boyd, D. B., Eds.; VCH: New York, 1991; pp 313−365.

(41) Boone, A. J.; Cory, M. G.; Scott, M. J.; Zerner, M. C.; Richards, N. G. J. *Inorg. Chem.* **2001**, *40*, 1837−1845.

(42) (a) Estiú, G. L.; Cory, M. G.; Zerner, M. C. *J. Phys. Chem. A* **2000**, *104*, 233−242. (b) Stavrev, K. K.; Urahata, S.; Herz, T.; Han, J.; Coucouvanis, D. *Int. J. Quantum Chem.* **2001**, *85*, 469−474. (c) Cory, M. G.; Stavrev, K. K.; Zerner, M. C. *Adv. Quantum Chem.* **1999**, *35*, 357−369. (d) Clark, T.*THEOCHEM* **2000**, *530*, 1−10.

Table 3. Structural Properties of the Initial and BLYP/6-31G* Optimized Geometries for Fe (III) Complexes **1**−**6**[a]

	internal coordinate	initial value[b]	$M_S = 1/2$	$M_S = 3/2$	$M_S = 5/2$		internal coordinate	initial value[b,c]	$M_S = 1/2$	$M_S = 3/2$
1	Fe−S1	2.196	2.22	2.21	2.35	**4**	Fe−S1	2.227	2.29	*d*
	Fe−S2	2.209	2.28	2.48	2.48		Fe−S2	2.230	2.29	*d*
	Fe−N1	1.978	1.98	2.18	2.17		Fe−N1	1.955	1.97	*d*
	Fe−N2	2.158	2.19	2.13	2.37		Fe−N2	1.998	1.98	*d*
	Fe−N3	1.969	1.97	2.12	2.17		Fe−N3	2.003	1.98	*d*
	Fe−N_{azide}	2.061	2.04	2.03	2.06		Fe−N4	1.955	1.97	*d*
	S1−Fe−N2	172.5	170.5	174.9	172.7		S1−Fe−N2	165.8	167.2	*d*
	N1−Fe−N3	174.9	174.3	167.5	167.2		S2−Fe−N3	166.7	167.0	*d*
							N1−Fe−N4	178.8	179.2	*d*
2	Fe−Cl	2.336	2.26	2.31	2.25	**5**	Fe−S1	2.198	*d*	2.22
	Fe−S1	2.195	2.22	2.27	2.37		Fe−S2	2.197	*d*	2.22
	Fe−S2	2.187	2.23	2.25	2.37		Fe−N1	2.227	*d*	2.33
	Fe−N1	1.980	1.95	1.99	2.15		Fe−N2	2.023	*d*	2.03
	Fe−N2	2.031	1.96	2.02	2.15		Fe−N3	2.021	*d*	2.03
	S1−Fe−S2	82.3	84.2	84.3	88.7		Fe−N4	2.228	*d*	2.33
	N1−Fe−N2	83.4	85.1	83.9	78.7		S1−Fe−S2	90.1	*d*	91.2
							N1−Fe−N4	151.1	*d*	151.8
3	Fe−S1	2.308	2.23	2.31	2.36					
	Fe−S2	2.302	2.24	2.36	2.35	**6**	Fe−S1	2.287	2.316	*d*
	Fe−S3	2.294	2.22	2.39	2.34		Fe−S2	2.270	2.311	*d*
	Fe−N1	2.211	2.07	2.04	2.38		Fe−S3	2.286	2.343	*d*
	Fe−N2	2.145	2.02	2.03	2.24		Fe−N1	2.075	2.153	*d*
	S1−Fe−S2	125.6	127.1	124.3	122.9		Fe−N2	2.058	2.151	*d*
	N1−Fe−N2	176.7	176.7	177.2	176.9		Fe−N3	2.080	2.139	*d*

[a] Atom labels correspond to those shown in Figure 1. [b] Bond lengths and angles are those of the initial structure used in the DFT calculations, which may differ very slightly from the crystal structure (see Table S1 in Supporting Information). All bond distances and angles are reported in units of Å and deg, respectively. [c] Values for the initial geometry of **5** are reported for its high temperature (295 K) structure. [d] The DFT-optimized geometry of the complex at this spin state was not computed.

Overall, the DFT wave functions for Fe(III)-containing complexes **1**−**6**, obtained using either the B3LYP or BLYP functionals at the observed geometries, suffer from limited spin contamination, based on the noninteracting values of $\langle S^2 \rangle_{KS}$ computed in *Gaussian98* (Table 2). For example, the B3LYP wave functions for the doublet states of complexes **2** and **3** exhibited significant amounts of spin contamination. Since **2** and **3** exhibit ground state quartet and sextet spin configurations, respectively, at their crystal geometries, it is reasonable that the calculated doublet Kohn−Sham wave functions will become spin contaminated as the spatial overlap of α and β orbitals decreases to more closely resemble a lower M_S determinant of a higher S state, in this case $M_S = 1/2$.[43]

Energetics and Structural Properties of Complexes 1−3 at Their Spin-State-Dependent DFT-Optimized Geometries. Having established the overall ability of DFT calculations to reproduce the ground state spin multiplicity for complexes **1**−**6** at their experimental geometries, we investigated the ability of DFT methods to (i) reproduce these geometries *a priori*, and (ii) model the relationship between electronic and molecular structure in these Fe(III)-containing compounds. Geometry optimization was carried out for complexes **1**−**3** at each of their three possible spin states, and for **4**−**6** at their experimentally determined spin state. In general, the optimized structures corresponding to the known ground state spin and the experimental structures were very similar, as judged by both numerical (Table 3) and graphical comparisons (Figure 3). The increased bond lengths between the axial nitrogen ligands and Fe(III) in the optimized structure of **5** at the quartet versus the doublet spin state are in excellent agreement with those seen in the structure of the high temperature (295 K) form. On the other hand, the DFT-optimized structure of **3** at its preferred sextet spin state appears to differ significantly from experiment. For example, the Fe−N bonds of the optimized high spin ($M_S = 5/2$) structure are longer than those observed in the crystal, and the pucker of the rings containing the metal−ligand bonds is noticeably different in the theoretical and experimental structures (Figure 3, see **3C**). Examination of the unit cell, however, suggested that crystal packing likely influences the experimental geometry observed for the rings of the ligand in complex **3**.

Correlations between metal−ligand bond lengths, molecular symmetry, and Fe(III) spin state, at least as expected from qualitative arguments of electrostatic repulsion between ligand electrons and metal d-orbitals, were also reproduced by these DFT geometry optimizations, with changes in bond lengths and angles being greater than the uncertainty of the computational method. For example, the Fe(III)−ligand bond lengths computed for complex **1** in the $M_S = 5/2$ state are significantly longer than those observed at its actual low spin ground state (Table 3). Longer metal−ligand bonds, as well as the distortion in the N1−Fe−N3 bond angle, should

(43) A true spin doublet ($S = 1/2$) has only one unpaired electron. In a spin-unrestricted *ansatz*, and to the degree that essentially paired α- and β spin orbitals unpair in space, a single determinant belonging to a higher spin state with the same M_S value is approximated. For example, a quantum mechanically rigorous description of a system with quantum numbers $|S,M_S\rangle = |5/2,1/2\rangle$ requires a linear combination of multiple determinants to take into account the 10 ways of arranging three α- and two β spin electrons in five unique spatial orbitals. Nevertheless, within the limitation of a single-determinant wave function, a particular spin configuration associated with a specific determinant can be intuitively mapped to a $|S,M_S\rangle$ state of broken spatial symmetry. More detailed discussions of these issues are available: (a) Noodleman, L.; Case, D. A. *Adv. Inorg. Chem.* **1992**, *38*, 423−470. (b) Koch, W.; Holthausen, M. C. *A Chemist's Guide to Density Functional Theory*, 2nd ed.; Wiley-VCH: Weinheim, 2001; pp 149−155.

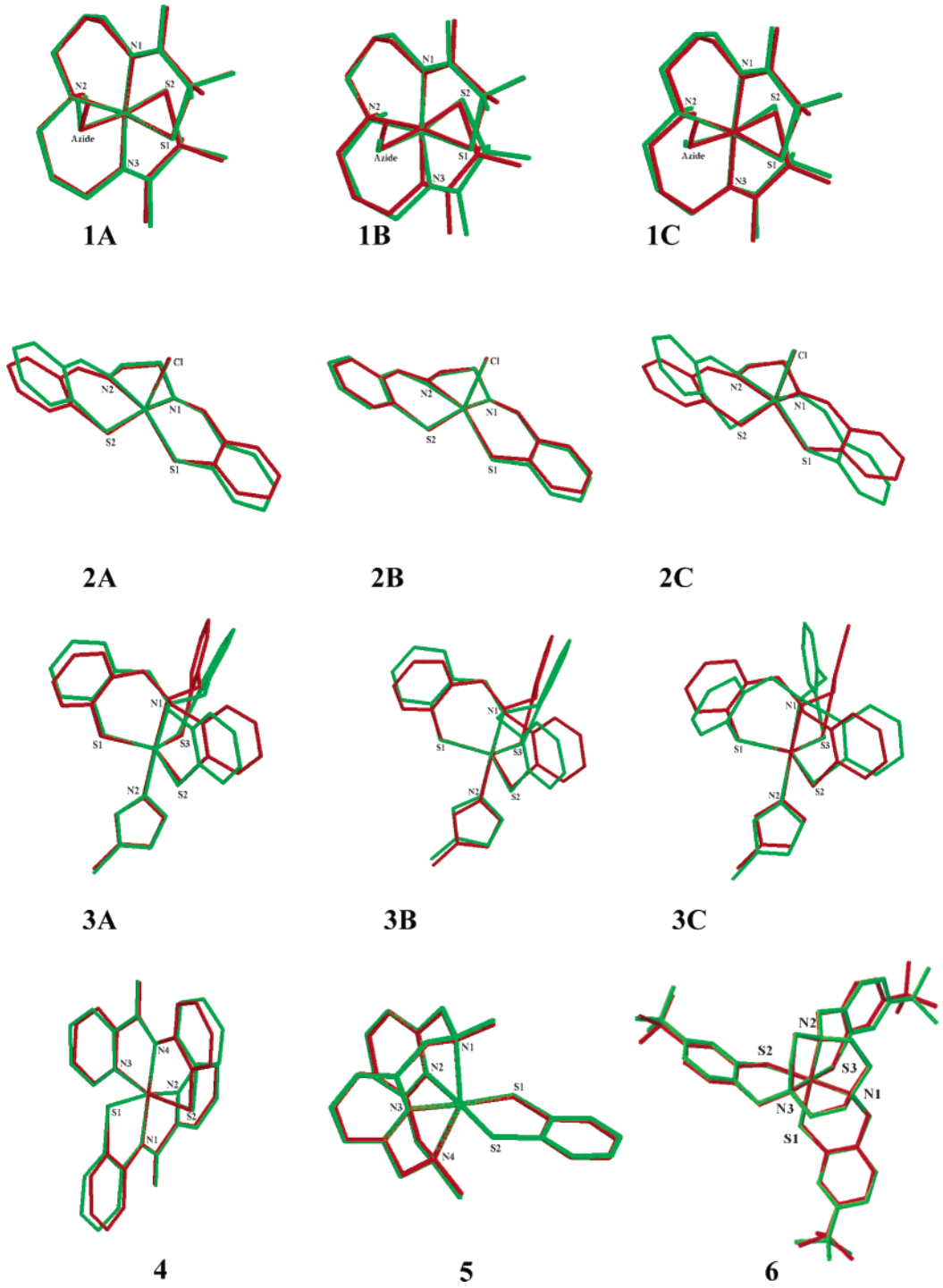

Figure 3. Superimposition of spin state specific DFT-optimized geometries and initial structures of Fe(III) complexes **1**−**6**. Structures are colored using the following scheme: initial structure, red; optimized structure, green. In the case of **5**, the crystal structure obtained at 295 K is shown in the superimposition. Complexes were optimized at the following spin multiplicities: **1A**, $M_S = 1/2$; **1B**, $M_S = 3/2$; **1C**, $M_S = 5/2$; **2A**, $M_S = 1/2$; **2B**, $M_S = 3/2$; **2C**, $M_S = 5/2$; **3A**, $M_S = 1/2$; **3B**, $M_S = 3/2$; **3C**, $M_S = 5/2$; **4**, $M_S = 1/2$; **5**, $M_S = 3/2$; **6**, $M_S = 1/2$.

decrease the splitting of the metal d orbitals, thereby stabilizing the high spin state. When complex **1** was optimized at its intermediate, quartet spin state, the axial Fe−N1 and Fe−N3 bonds lengthened by up to 0.20 Å from the initial structure, and distortion of the N1−Fe−N3 bond angle was observed (Table 3). Presumably, orbital degeneracy is removed as a consequence of these changes in geometry thereby allowing the adoption of a low energy quartet electronic configuration. The average magnitude (approximately 0.18 Å) of the calculated changes in metal−ligand bond lengths in the octahedral complex **1** in its various spin states is consistent with experimental observations. For example, in Fe(III) complexes that undergo spin crossover, the average bond lengths for the experimental low spin ($M_S = 1/2$) and high spin ($M_S = 5/2$) geometries have been shown to change by approximately 0.15 Å.[44]

In the case of the square pyramidal Fe(III) complex **2**, shortening the axial Fe−Cl bond (positioned along the *z*-axis)

might be expected to raise the energy of the a_1 orbital in a simple electrostatic d-shell repulsion model, while the lengthening of the remaining ligand bonds would lower the b_1 and b_2 orbital energies as well as the a_1 energy (Scheme S1, Supporting Information). The net result of both changes should compress the energy range of the d-orbital manifold, resulting in a high spin multiplicity. Geometrical changes from the experimental structures that are consistent with this model are observed in the calculated, optimized geometries for complex **2** at the intermediate and high spin states (Table 3). Equally, shortening the Fe−Cl bond without any changes in the remaining metal−ligand bond lengths should raise the energy of a_1 orbital, thereby increasing the energetic splitting of the b_2 and a_1 orbitals and leading to a stabilization of the low spin electronic configuration. Consideration of the DFT-optimized structures of **2** reveals small decreases in both the axial Fe−Cl and the equatorial metal−ligand bond lengths in the doublet structure relative to their values in the BLYP-optimized quartet. Although the Fe−S bond lengths in the BLYP-optimized structure of **2** at the quartet state were longer than those seen in the initial geometry, we note that one of the two independent molecules that are present in the unit cell has slightly longer Fe−S bonds than the other.[24] This observation suggests that crystal packing effects may explain this small discrepancy between theory and experiment.

The axial Fe−N1 and Fe−N2 bond lengths of complex **3**, as calculated for an excited state spin quartet, decreased significantly (0.34 and 0.21 Å, respectively) relative to the cognate bonds at the optimized sextet geometry. This behavior is again consistent with that expected from qualitative ligand field models in which increased axial metal−ligand interactions in a trigonal bipyramidal complex would raise the a_1' orbital energy to increase the splitting between the e′ and a_1' orbitals (Scheme S2, Supporting Information). When optimized at the low spin state, the decrease in the axial Fe−N bond lengths relative to their values in the high spin structure was accompanied by concomitant shortening of the remaining metal−ligand bonds. The trigonal arrangement of the equatorial ligands was also distorted due to an increase in the S1−Fe−S2 bond angle (Figure 3, see **3A**). The latter observation is consistent with expectations from the Jahn−Teller theorem, in which the symmetry of a system will break in order to remove orbital degeneracy resulting in maximal occupancy of the two lowest energy molecular orbitals.

Given that BLYP-optimized geometries for complexes **1**−**3** at their three possible spin states were available, we next determined whether DFT calculations employing the B3LYP functional would give relative energies for these structures that were consistent with known ground spin states from experimental measurements (Table 4). Calculations using the B3LYP functional reproduced the known ground spin state of these complexes, although the difference between the quartet and sextet state energies computed for complex **2** is within the known uncertainty of the method. In addition, the noninteracting $\langle S^2\rangle_{KS}$ values showed a marked improvement in the level of spin contamination for the low spin state B3LYP wave functions of **2** and **3** relative to that seen for calculations of vertical transition energies. On the other hand, single point energies computed at these optimized geometries using the BLYP functional predicted that complex **3** should adopt a doublet or quartet rather than the observed sextet state. The ordering of spin states using the BLYP and B3LYP models was also completely different for the three complexes, with BLYP stabilizing determinants of lower spin multiplicity (Table 4).

Table 4. Relative Spin State Energies and Noninteracting $\langle S^2\rangle_{KS}$ Values Calculated for Fe(III) Complexes **1**−**6** at their BLYP/6-31G* Optimized Geometries[a]

	BLYP/6-31G*			B3LYP/6-31G*		
complex	energy (cm^{-1})	$\langle S^2\rangle_{KS}$[b]	$2S+1$	energy (cm^{-1})	$\langle S^2\rangle_{KS}$[b]	$2S+1$
			1 (Doublet)			
$M_S = 1/2$	0	0.76	2.01	0	0.77	2.02
$M_S = 3/2$	5184	3.81	4.03	1961	3.88	4.06
$M_S = 5/2$	7664	8.76	6.00	1627	8.76	6.00
			2 (Quartet)			
$M_S = 1/2$	1656	1.02	2.25	5208	1.23	2.43
$M_S = 3/2$	0	3.80	4.02	0	3.84	4.04
$M_S = 5/2$	2799	8.76	6.00	353	8.76	6.00
			3 (Sextet)			
$M_S = 1/2$	*0*	0.76	2.01	4246	0.91	2.15
$M_S = 3/2$	*714*	3.79	4.02	1739	3.83	4.04
$M_S = 5/2$	*1289*	8.76	6.00	0	8.76	6.00

[a] Results from calculations that identify the incorrect ground spin state are italicized. [b] $2S + 1 = (4\langle S^2\rangle_{KS} + 1)^{1/2}$.

Chemical Bonding in the DFT-Optimized, Ground State Structures of Complexes 1−6. The extent to which coordination of Fe(III) by deprotonated amides plays a role in determining the spin state properties and reactivity of the NHase metal center, as well as in inorganic model complexes, remains a subject of discussion.[4a,45] Similar metal−amide bonds in metalloenzymes are rare, the only other examples being observed in nitrogenase[46] and acetyl-CoA synthase/carbon monoxide dehydrogenase.[47] In light of the ability of DFT calculations employing the B3LYP functional to model the observed spin states and optimized geometries of Fe(III) complexes **1**−**6**, we undertook a detailed analysis of the B3LYP wave function, as represented by a single determinant of Kohn−Sham orbitals, within the NBO formalism for each structure at its ground state, BLYP-optimized geometry. Our initial analysis examined the distribution of electrons in these complexes, as determined by spin magnetization density (SMD) and partial charges obtained using natural population analysis (NPA) (Table

(44) König, E. In *Structure and Bonding*; Clarke, M. J., Goodenough, J. B., Ibers, J. A., Jørgensen, C. K., Mingos, D. M. P., Neilands, J. B., Palmer, G. A., Reinen, D., Sadler, P. J., Weiss, R., Williams, R. J. P., Eds.; Springer-Verlag: Berlin, 1991; Vol. 76, pp 51−152.

(45) Shearer, J.; Jackson, H. L.; Schweitzer, D.; Rittenberg, D. K.; Leavy, T. M.; Kaminsky, W.; Scarrow, R. C.; Kovacs, J. A. *J. Am. Chem. Soc.* **2002**, *124*, 11417−11428.

(46) Smith, B. E. *Adv. Inorg. Chem.* **1999**, *47*, 159−218. (b) Peters, J. W.; Stowell, M. H. B.; Soltis, S. M.; Finnegan, M. G.; Johnson, M. K.; Rees, D. C. *Biochemistry* **1997**, *36*, 1181−1187.

(47) (a) Darnault, C.; Volbeda, A.; Kim, E. J.; Legrand, P.; Vernède, X.; Lindahl, P. A.; Fontecilla-Camps, J. C. *Nat. Struct. Biol.* **2003**, *10*, 271−279. (b) Doukov, T. I.; Iverson, T. M.; Seravalli, J.; Ragsdale, S. W.; Drennan, C. L. *Science* **2002**, *298*, 567−572.

Table 5. NPA-Derived Partial Charges and Spin Magnetization Densities (SMDs) of Selected Atoms in Fe(III) Complexes **1**−**6** at Their DFT-Optimized Geometries[a,b]

	atom	partial charge	SMD		atom	partial charge	SMD
^{2}**1**	Fe	+1.38	+1.052	^{2}**4**	Fe	+1.34	+1.002
	S1	−0.28	+0.013		S1	−0.24	+0.008
	S2	−0.39	−0.011		S2	−0.24	+0.009
	N1	−0.53	−0.012		N1	−0.68	−0.006
	N2	−0.72	−0.006		N2	−0.49	−0.006
	N3	−0.52	−0.011		N3	−0.50	−0.006
	N_{azide}	−0.65	−0.012		N4	−0.68	−0.006
					O1	−0.67	+0.001
					O2	−0.67	+0.001
^{4}**2**	Fe	+1.48	+2.850	^{4}**5**	Fe	+1.52	2.909
	Cl	−0.69	+0.195		S1	−0.27	−0.020
	S1	−0.21	−0.019		S2	−0.27	−0.020
	S2	−0.18	−0.048		N1	−0.55	+0.061
	N1	−0.58	−0.030		N2	−0.56	−0.001
	N2	−0.59	−0.005		N3	−0.56	−0.001
					N4	−0.55	+0.062
^{6}**3**	Fe	+1.66	+4.073	^{2}**6**	Fe	+0.73	+1.190
	S1	−0.42	+0.207		S1	−0.14	−0.073
	S2	−0.38	+0.239		S2	−0.12	−0.035
	S3	−0.39	+0.240		S3	−0.13	−0.054
	N1	−0.55	+0.074		N1	−0.52	−0.015
	N2	−0.62	+0.059		N2	−0.52	−0.010
					N3	−0.52	−0.011

[a] Atom labels correspond to those shown in Figure 1. [b] Observed spin multiplicities are shown as superscripts.

5).[15,48] The metal center carried a partial positive charge in all complexes, values ranging from +0.73|e$^-$| (complex **6**) to +1.66|e$^-$| (complex **3**) even though the metal is formally in the ferric oxidation state. The reduced Fe(III) charges can likely be attributed to the nephelauxetic effect, whereby ligand charge donation partially shields the metal d electrons from the central ion nuclear charge and drives expansion of the d-electron "cloud".[49] The identity of the metal as Fe(III) was more clearly evident from the SMD computed for each complex. In all cases but that of complex **3**, the excess α spin on the iron was within 0.2 units of formal expectation for a d^5 system (Table 5). For complex **3**, SMD analysis revealed the presence of significant spin delocalization onto the sulfur atoms coordinating the Fe(III), but even so approximately 97% of the spin density was located within the first sphere of ligand atoms (Figure 4). This spin delocalization likely results from the polarizability of sulfur ligands and the high spin configuration adopted by Fe(III) in the electronic ground state of this complex. Visualization of the SMD for complexes **1**−**6** (Figure 4) showed that there is little uncompensated β spin density in the wave functions calculated for these structures, consistent with the modest spin contamination as measured by the deviation of $\langle S^2\rangle_{KS}$ from $M_S \cdot (M_S + 1)$ (Table 3). The absence of uncompensated β spin density in these visualizations also signals that the wave function is a reasonable single-determinant approximation to a state of "pure" spin in which occupation of the Kohn−Sham molecular orbitals reflects broken spatial symmetry.

In an effort to probe the extent of covalency in the Fe−ligand bonds of complexes **1**−**6**, bond orders were computed using the natural atomic orbital (NAO) compositions of natural localized molecular orbitals (NLMOs), with the sign of these values being obtained from the overlap integrals between natural hybrid orbitals (NHOs) located on the covalently bonded atoms (Table 6). Such NPA/NLMO bond orders[50] have been considered to be superior to alternative metrics[15b] and have been applied in analyses of the extent of d-orbital participation in the bonding of main-group complexes.[50] In spin-unrestricted calculations, which have separate α spin and β spin density matrices, we consider the total bond order to be the sum of α- and β spin bond orders, and the difference between these values to represent the extent of spin polarization in the bond, at least within a single-reference approximation. Across the series of six complexes, the Fe−S bonds tend to show a greater degree of σ covalency than those between the metal and first-row elements, and only small amounts of bond spin polarization are observed in **1**, **4**, and **6**, which have ground state doublet configurations. The bond between Fe and the azide nitrogen in **1** shows the greatest degree of "relative" spin polarization at 17%, while the most polarized bonds of **4** and **6** are Fe−N4 and Fe−S1, respectively. Complexes **2** and **5** have several bonds with large (∼70%) amounts of relative spin polarization, although only the Fe−Cl bond in **2** is significantly polarized in absolute terms, with almost 0.2 |e$^-$| more β than α spin character. Every metal−ligand bond in sextet complex **3** is spin-polarized to an extent of 60−70%, which is consistent with an excess of nonbonding α spin electrons localized on Fe: Pauli repulsion keeps ligand α-electrons further away from the metal than β-electrons.

For all six complexes, a clear trend is also seen in the total bond order between Fe(III) and its ligands compared with the molecular spin state (Table 6). Thus, the doublet state of **6** has a total bond order of 2.03, a value greater than that computed for **1** and **4** (approximately 1.7), which are also ground state doublets. All three total bond orders exceed the values of 1.21 and about 1.55 that are calculated for the sextet complex **3**, and quartet complexes **2** and **5**, respectively. Given that the latter two compounds have different coordination (Table 1), the similarity in computed total metal bond order is especially noteworthy. As an alternative approach to exploring the chemical bonding in these open-shell systems, we analyzed each of the ground state, optimized complexes using bond valence sum (BVS) analysis.[51] These calculations employed known parameters for N and S ligands bonded to Fe(III),[51a] and a reference length of 1.976 Å for the Fe−Cl bond calculated according to literature procedures.[51b] In agreement with our NBO-based strategy, the BVS values calculated for complexes **2** and **5** were similar despite the different Fe coordination numbers. In addition, bond valence sums were inversely related to the

(48) Reed, A. E.; Weinstock, R. B.; Weinhold, F. *J. Chem. Phys.* **1985**, *83*, 735−746.
(49) Schäffer, C. E. *Inorg. Chim. Acta* **2000**, *302*, 1035−1076.
(50) Reed, A. E.; Schleyer, P. v. R. *J. Am. Chem. Soc.* **1990**, *112*, 1434−1445.
(51) (a) Liu, W.; Thorp, H. H. *Inorg. Chem.* **1993**, *32*, 4102−4105. (b) Brown, I. D.; Altermatt, D. *Acta Crystallogr., Sect. B* **1985**, *41*, 244−247.

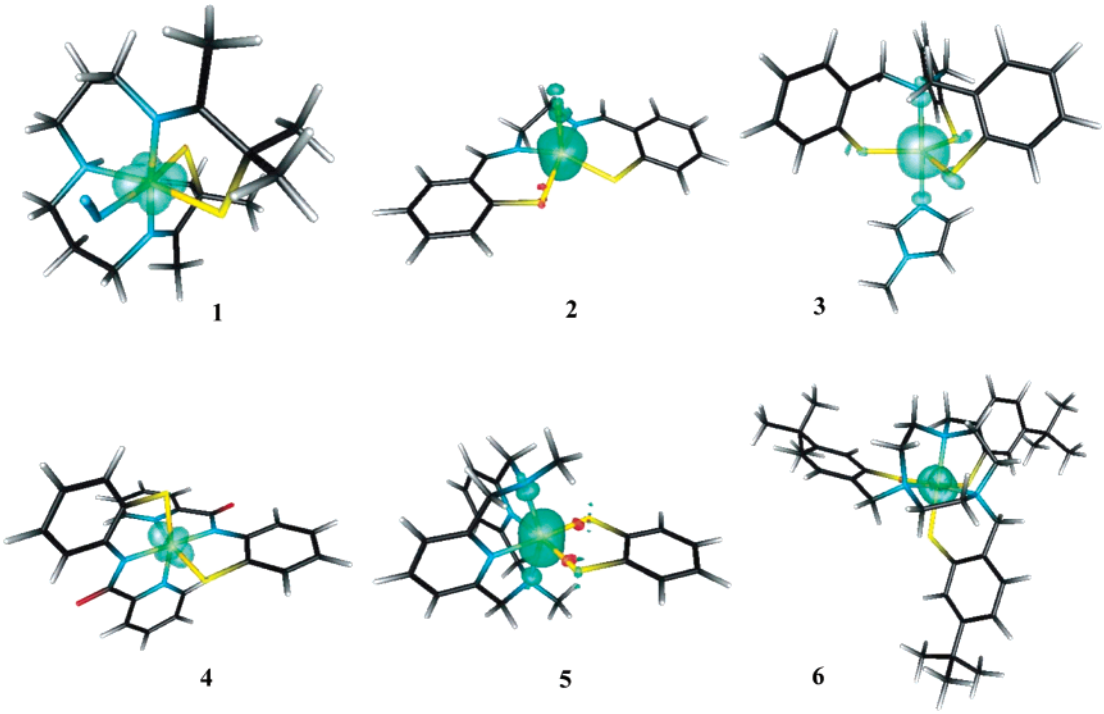

Figure 4. Graphical representations of the spin magnetization density computed for the DFT-optimized structures of Fe(III) complexes **1**−**6**. Positive density is contoured as green, negative as red. Atoms are colored using the following scheme: C, black; H, white; N, blue; O, red; S, yellow; Fe, orange; Cl, green.

spin magnitude observed for these complexes at their experimental geometries (Table S2, Supporting Information). In contrast, while the assumption of equality between the BVS and the formal valence of the metal center appears justified for **2**, **5**, and **6**, it does not hold for the low spin complexes **1** and **4** (BVS > 3) and the sextet **3** (BVS < 3). The apparent failure of BVS calculations for these systems likely reflects the fact that effects arising from spin configuration were not explicitly included in the original formulation of this method. The uniform decrease in BVS upon DFT optimization of the experimental structures is consistent with the general lengthening of the Fe−ligand bonds associated with the BLYP functional,[43b] but the cause of the disproportionate drop in the BVS value for complex **6** upon optimization is unclear. Although the BVS-valence equivalence appears to be violated in our test set, it is clearly possible that BVS analysis on crystallographic structures of known valence, and NPA/NLMO bond orders computed for molecules resembling **1**−**6** at their optimized geometries, might be equally valuable strategies in predicting spin multiplicities.

Analysis of Metal−Ligand Covalency in the Ground State Structures of Complexes 1−6. Estimating the extent of covalency for metal−ligand bonds in open-shell transition metal complexes on the basis of bond order will be dependent on the particular choice of metric, for which there are many possible definitions.[15b] Such information, however, is likely to be an important element in assigning the relative roles of Fe−S and Fe−amide bonding for determining the low spin ground state of the NHase metal center.[4a,45] Although the NPA/NLMO bond orders computed for **1**−**6** were consistent with the expectation that bonds between Fe and polarizable ligands have a greater order than those between Fe and "hard" ligands, we nevertheless sought to develop a systematic analysis of the NBO data that would (i) estimate covalency in terms of electrons shared, and (ii) allow partitioning into different symmetries of metal−ligand interaction. Interactions that may be considered in the description of metal−ligand bonding include pure ionicity (crystal-field), σ-overlap, π-back-bonding, and π-donation. The analysis of NPA partial charges and NPA/NLMO bond orders, together with comparisons of NBOs and their corresponding NLMOs, can be used to estimate the contribution of each type of interaction to metal−ligand bonding. The utility of comparing NBOs with NLMOs to estimate covalency in metal−ligand bonding, particularly in distinguishing σ- from π-symmetry interactions, has been recognized.[52] The combination of this idea, NBOs, and three-centered hyperbonding leads to a formalized yet intuitive strategy for the analysis of metal−ligand bonding. Purely ionic interactions are outside the scope of the method as applied in this paper. Fe−ligand bonds with covalent character greater than a threshold value, which is dynamically adjusted in the NBO method until a suitable reference Lewis structure is found, will appear as NBOs. The NHO composition of all Fe-contributing NBOs in the six DFT-optimized complexes was identified using the algorithms implemented in NBO v5.0. In our analysis of complexes **1**−**6**, these NBOs were invariably σ-bonds: no π-symmetry metal−ligand interaction was sufficiently strong to appear as a NBO. For all complexes, the primary NHO located on Fe that participated in covalent bonding was of an sd^n type, with the contribution of the Fe 4s orbital varying widely between 15% and 53% (Table 7). On the other hand, ligand orbitals

(52) Kaupp, M. *Chem. Eur. J.* **1999**, *5*, 3631−3643.

Table 6. Selected NLMO/NPA Bond Orders in Fe(III) Complexes **1**−**6** at Their DFT-Optimized Geometries[a,b]

	bond	α spin order	β spin order	α + β	total metal bond order	α − β	[(α − β)/(α + β)] × 100[a]
1	Fe−S1	0.278	0.285	0.563	1.702	−0.007	−1.2
	Fe−S2	0.224	0.199	0.422		+0.025	+5.8
	Fe−N1	0.112	0.092	0.204		+0.020	+9.7
	Fe−N2	0.048	0.047	0.095		+0.000	+0.4
	Fe−N3	0.101	0.085	0.186		+0.016	+8.4
	Fe−N_{azide}	0.096	0.136	0.232		−0.040	−17.0
2	Fe−Cl	0.041	0.239	0.279	1.544	−0.198	−70.9
	Fe−S1	0.236	0.196	0.433		+0.040	+9.2
	Fe−S2	0.268	0.220	0.488		+0.048	+9.8
	Fe−N1	0.078	0.104	0.181		−0.026	−14.3
	Fe−N2	0.067	0.096	0.163		−0.029	−18.0
3	Fe−S1	0.059	0.270	0.329	1.213	−0.212	−64.3
	Fe−S2	0.054	0.300	0.355		−0.246	−69.3
	Fe−S3	0.062	0.297	0.358		−0.235	−65.6
	Fe−N1	0.016	0.070	0.087		−0.054	−62.0
	Fe−N2	0.015	0.068	0.084		−0.053	−63.6
4	Fe−S1	0.235	0.207	0.441	1.738	+0.028	+6.4
	Fe−S2	0.235	0.248	0.483		−0.013	−2.7
	Fe−N1	0.106	0.126	0.233		−0.020	−8.5
	Fe−N2	0.079	0.090	0.169		−0.010	−6.0
	Fe−N3	0.079	0.090	0.170		−0.011	−6.6
	Fe−N4	0.106	0.136	0.242		−0.029	−12.2
	N1−C(O)	0.510	0.506	1.016		+0.004	+0.4
	N4−C(O)	0.510	0.506	1.016		+0.004	+0.34
	C(O)−O1	0.609	0.611	1.220		−0.002	−0.18
	C(O)−O2	0.609	0.611	1.220		−0.002	−0.14
5	Fe−S1	0.298	0.260	0.557	1.564	0.038	+6.8
	Fe−S2	0.297	0.298	0.595		0.000	−0.07
	Fe−N1	0.011	0.067	0.078		−0.056	−72.1
	Fe−N2	0.060	0.073	0.133		−0.012	−9.2
	Fe−N3	0.060	0.068	0.128		−0.008	−5.9
	Fe−N4	0.010	0.063	0.073		−0.052	−71.3
6	Fe−S1	0.311	0.228	0.539	2.027	0.083	+15.3
	Fe−S2	0.293	0.255	0.548		0.038	+7.0
	Fe−S3	0.300	0.252	0.552		0.047	+8.6
	Fe−N1	0.062	0.066	0.128		−0.005	−3.6
	Fe−N2	0.065	0.069	0.134		−0.004	−3.1
	Fe−N3	0.060	0.067	0.126		−0.007	−5.5

[a] Atom labels correspond to those shown in Figure 1. [b] Percentages are calculated using α- and β-bond orders of higher precision than shown in the table.

participating in covalent bonding the Fe in these complexes had mostly p character, ranging from 50% to 96%, with d-orbital contributions from sulfur ligands being less than 1%. NBO surface plots demonstrate the σ-symmetry of these NBOs, and the variety of bonds between Fe and ligand atoms that were found to be highly covalent (Figure 5). NBO analysis was also used to identify three-center "hyperbonding",[15] which we interpret as the participation of a significant resonance structure involving the interaction of a lone-pair on one ligand atom and the formal NBO between Fe(III) and another ligand atom (usually sulfur). Three-center hyperbonding that enhanced the degree of covalency in Fe−N bonds at the expense of Fe−S bonds was observed in complexes **1**, **2**, **4**, and **6**. On the basis of the symmetry of the participating NBOs, the increase in covalency was primarily associated with σ-donation by the N atom.

In addition to the NBOs automatically identified by the software algorithms, three types of metal−ligand interactions remain to be considered: σ-donation by ligand lone electron pairs of a degree less than the threshold defining an NBO; π-donation by ligands to the metal; and π-back-bonding from metal to ligand. The differential properties of NBOs and NLMOs are valuable in deriving the contributions of these interactions to ground state metal−ligand bonding. Thus, NBOs emphasize spatial locality at the expense of occupation number: they are defined over at most two atomic centers, and their occupations deviate below 1.00 (for a spin−orbital basis) in proportion to the delocalization of the electron into empty orbitals elsewhere in the molecule. NLMOs, on the other hand, have integral occupation numbers by construction, although they are usually still associated with a particular NBO. What may be thought of as the "additional" fractional electron as one moves conceptually from an NBO to an NLMO comes from the principal delocalizations of the NBO within the NHO basis. In effect, the NLMO is the deviation of reality from an idealized local bonding picture. The different compositions between an NBO and its corresponding NLMO are thereby well suited to extract the degree to which electrons in a crystal-field model of a metal complex, e.g., $d^{5.0}$ Fe^{3+}, with ligands of integral charge, delocalize weakly between the metal and ligands to produce covalency. For example, metal-to-ligand donation appears as ligand lone pair hybrid character in a d-type metal NLMO that was not present in the associated NBO. Likewise, systematic examination of the Fe character in ligand LP NLMOs reveals the extent to which ligand charge has moved into the metal center relative to a localized NBO reference.[53] Illustrations of these ideas are provided by several NBO-NLMO pairs taken from an analysis of the Kohn−Sham wave function for complex **2** (Figure 6). Hence a mostly LP

Table 7. NHO Compositions of NBOs Containing Fe Character in Fe(III) Complexes **1**−**6** at Their DFT-Optimized Geometries[a]

	NBO	occupancy	Fe character (%)	Fe hybridization	ligand hybridization
1	α Fe−S1	0.96643	27.0	$sd^{2.2}$	sp^{15}
	β Fe−S1	0.97283	21.7	$sd^{3.4}$	sp^{11}
	α Fe−S2	0.96505	22.8	$sd^{1.9}$	sp^{15}
	α Fe−N1	0.97256	11.3	$sd^{1.9}$	$sp^{3.1}$
	β Fe−N_{azide}	0.80365	14.7	$sd^{5.1}$	sp
2	α Fe−S1	0.95094	23.1	$sd^{0.9}$	sp^{16}
	α Fe−S2	0.94614	26.4	$sd^{1.2}$	sp^{18}
3	β Fe−S1	0.96942	21.8	$sp^{0.1}d^{5.5}$	$sp^{25}d^{0.1}$
	β Fe−S2	0.96960	23.4	$sp^{0.1}d^{5.4}$	$sp^{25}d^{0.1}$
	β Fe−S3	0.97160	23.7	$sd^{4.7}$	$sp^{26}d^{0.1}$
4	α Fe−S1	0.97308	24.5	$sd^{3.8}$	sp^{14}
	α Fe−S2	0.97296	24.6	$sd^{3.8}$	sp^{14}
5	α Fe−S1	0.93891	27.7	sd	sp^{17}
	α Fe−S2	0.93889	27.7	sd	sp^{17}
6	α Fe−S1	0.94634	31.5	$sd^{2.1}$	sp^{11}
	α Fe−S2	0.94202	31.3	$sd^{1.9}$	sp^{11}
	α Fe−S3	0.94426	31.4	$sd^{2.0}$	sp^{11}
	β Fe−S1	0.96339	21.4	$sd^{2.0}$	$sp^{6.9}$
	β Fe−S2	0.96238	22.6	$sd^{2.0}$	$sp^{7.3}$
	β Fe−S3	0.96480	21.6	$sd^{2.0}$	$sp^{6.6}$

[a] Atom labels correspond to those shown in Figure 1.

(53) We note that while the NBO algorithm analyzes α and β spin density matrices separately, we and the NBO program authors define a lone "pair" (LP) to signify a valence orbital localized essentially to a single atomic center, despite a maximum possible spin−orbital occupancy of 1.0.

(54) Murakami, T.; Nojiri, M.; Nakayama, H.; Odaka, M.; Yohda, M.; Dohmae, N.; Takio, K.; Nagamune, T.; Endo, I. *Protein Sci.* **2000**, *9*, 1024−1030.

(55) Wendt, M.; Weinhold, F. *NBOView 1.0*; Theoretical Chemistry Institute, University of Wisconsin: Madison, WI, 2001.

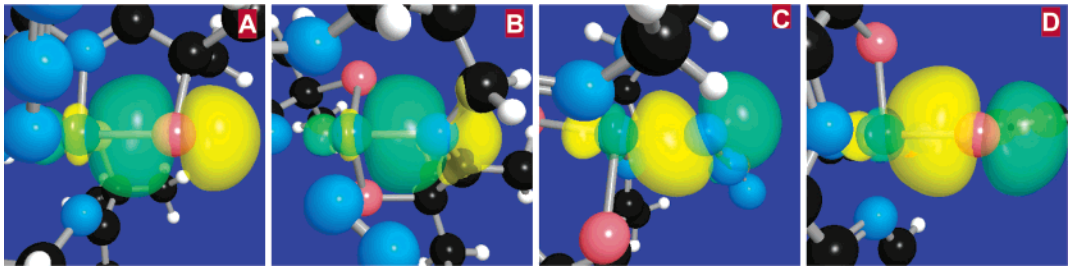

Figure 5. Spin NBOs exhibiting significant covalency in Fe−ligand bonds that are representative types present in complexes **1**−**6**: (A) **1**, α Fe−S1 (thiolato); (B) **1**, α Fe−N1; (C) **1**, β Fe−N_{azide}; (D) **4**, α Fe−S1 (thiophenolato). In all figures, Fe is located at the left end of the NBO, and orbitals are colored green and yellow to represent positive and negative phases, respectively. Atom labels correspond to those given in Figure 1.

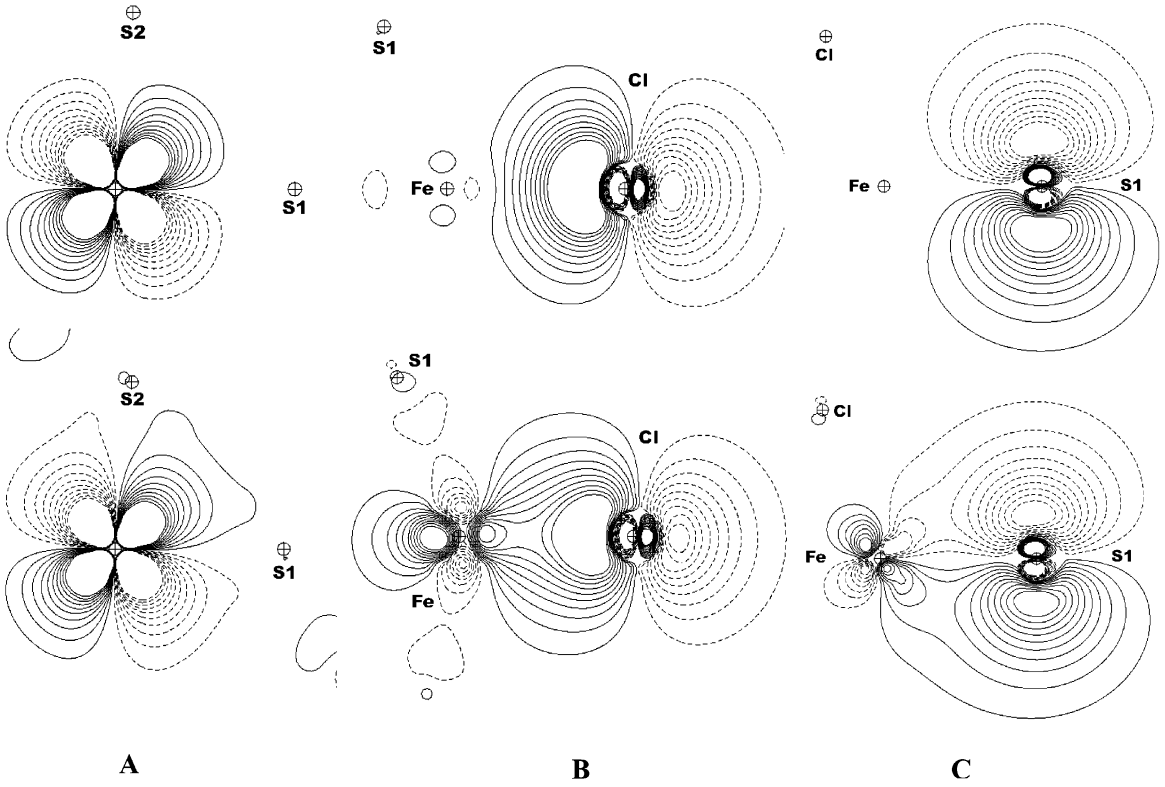

Figure 6. Selected NBOs (top) and their corresponding NLMOs (bottom) for complex **2**. These illustrate three classes of weak electron delocalization between Fe and ligand atoms: (A) metal-to-ligand π-back-bonding; (B) ligand-to-metal σ-donation; (C) ligand-to-metal π-donation. Contours were generated with NBOView 1.0,[55] using a minimum value of 0.02, and step size of 0.02. Atom labels correspond to those shown in Figure 1.

Fe NLMO shows π-back-bonding to the sulfur atoms (Figure 6A), which is manifested as a distortion of the Fe d-type LP NBO toward the S atoms. The extent of covalency (ligand to metal σ-donation) in the mostly ionic Fe−Cl bond can be also seen in a Cl LP NBO and NLMO that point along the Cl−Fe line of centers (Figure 6B). Finally, the π-symmetry overlap evident in the NLMO of Figure 6C when compared to its clearly LP-type sulfur NBO signifies this as a π-donation from the S ligand to the Fe(III) center.

In order to place these ideas onto a quantitative footing, we devised the following scheme for calculating the extent of covalency in the Fe−ligand bonds. The weak delocalizations in LP-type NLMOs can be quantitated by the following expression:

$$\left[\sum_{\text{Fe LP}} L_{\text{NLMO}} \times (1 - {}^{1}O_{\text{Fe}})\right] + \left[\sum_{\text{L LP}} \text{Fe}_{\text{NLMO}} \times (1 - {}^{1}O_{\text{L}})\right] \quad (1)$$

where the first and second terms are summed over the one-center (lone-pair) NBOs centered on Fe and the ligand atom of interest, respectively. ${}^{1}O_{\text{Fe}}$ is the occupancy of a one-center NBO on iron, and hence, $(1 - {}^{1}O_{\text{Fe}})$ represents the number of Fe electrons that are delocalized onto other atoms. ${}^{1}O_{\text{L}}$ is the corresponding occupancy of a one-center NBO on the ligand atom, and $(1 - {}^{1}O_{\text{L}})$ represents the number of ligand electrons located elsewhere. L_{NLMO} is the ligand character in the Fe LP NLMO divided by the total non-Fe character, and Fe_{NLMO} is the iron character in a L LP NLMO divided by the total non-L character. Given these definitions, it is seen that the terms of expression (1) estimate the delocalization of (i) Fe electrons onto the ligand, and (ii) ligand electrons onto Fe, respectively. These latter two quantities therefore represent the fraction of delocalized Fe electrons on a specific ligand atom and the fraction of delocalized ligand electrons on Fe, respectively. Covalency contributed

by two-centered NBOs that do not participate in three-centered hyperbonding was estimated using the expression

$$[\min(Fe_{NBO} \text{ or } L_{NBO}) \times {}^2O] \quad (2)$$

where Fe_{NBO} and L_{NBO} represent the fraction of Fe and ligand NHO contributions in a two-center NBO, respectively, and ^2O is the electron occupancy of the two-center NBO. If a given Fe−ligand NBO was identified as participating in a three-centered hyperbond, then our calculations replaced expression 2 with the following:

$$[NBO_{3CHB} \times \min(Fe_{NBO} \text{ or } L_{NBO}) \times {}^3O] \quad (3)$$

in which NBO_{3CHB} is the amount of two-center NBO character in the three-center hyperbond, ^3O is the electron occupancy of the three-center hyperbond, and the remaining terms are defined as above. In our analysis, three-center hyperbonds arose from resonance between an Fe−ligand NBO and a donor lone pair on another ligand not involved in a metal-containing two-centered NBO. The additional covalency between Fe and this lone pair arising from participation in the three-centered hyperbond was estimated using the expression

$$[{}^3D \times \min(Fe_{NBO} \text{ or } L_{NBO}) \times {}^3O] \quad (4)$$

where ^3D is the donor lone-pair character in the three-center hyperbond. We chose to use three-center hyperbonds in lieu of their constituent NBOs as a basis for calculating covalency because they should better reflect the intrinsic bonding present between Fe and both the donor and acceptor ligand atoms than the NBO and lone pair separately would. Expressions (2)−(4), which define the covalency due to α-bonding between ligands and metal, range between 0 and 0.5 for NBOs with an extreme of either metal or ligand character, or with equal participation of the two, respectively. For example, if summed over hypothetical α and β NBOs of unit occupancy (equivalently, perfectly localized two-center NLMOs) between Fe and a ligand with 50% atomic character each, a total of 1.0 would result. The number of shared electrons can be considered as twice this number. Auxiliary donation or π-back-bonding would add to the calculated covalency via expression 1 beyond the contributions from formal two- or three-centered bonding. Thus, these expressions provide a convenient means by which to compare bonding of ligands in the same complex, or between complexes.

Using this approach, as summarized in expressions 1−4, we calculated the covalent contributions to all Fe−ligand bonds in **1**−**6**, and the total covalency present in these complexes (Table 8). Our results clearly explain the low spin character of complex **6** in its ground state. This experimental observation is perplexing at first sight because there are no obvious "strong field" ligands present in **6**. Our procedure suggests that metal−ligand covalency is higher in **6** than in the other five Fe(III) complexes, a fact mirrored by its high NPA/NLMO Fe−ligand bond order. Further analysis revealed that there is an exceptional amount of three-center hyperbonding in complex **6** that arises from the *trans* relationship of three pairs of thiophenolato (acceptor NBO) and amino (donor) ligands. The extensive mixing of the metal d orbitals with both the sulfur and nitrogen ligand orbitals raises the energy of the participating d-orbitals relative to those not aligned along the bond axes, thereby splitting the d manifold on Fe and stabilizing the low spin configuration.

Table 8. Covalent Character of Fe−Ligand Bonds in Complexes **1**−**6** at Their Optimized Ground State Geometries[a]

	bond	bond covalency (|e⁻|)	total covalency (|e⁻|)
1	Fe−S1	0.565	2.142
	Fe−S2	0.625	
	Fe−N1	0.217	
	Fe−N2	0.101	
	Fe−N3	0.299	
	Fe−N_{azide}	0.335	
2	Fe−Cl	0.270	1.732
	Fe−S1	0.426	
	Fe−S2	0.554	
	Fe−N1	0.341	
	Fe−N2	0.140	
3	Fe−S1	0.346	1.281
	Fe−S2	0.372	
	Fe−S3	0.383	
	Fe−N1	0.098	
	Fe−N2	0.081	
4	Fe−S1	0.5445	2.163
	Fe−S2	0.5570	
	Fe−N1	0.2036	
	Fe−N2	0.3193	
	Fe−N3	0.3192	
	Fe−N4	0.2193	
5	Fe−S1	0.540	1.471
	Fe−S2	0.540	
	Fe−N1	0.078	
	Fe−N2	0.119	
	Fe−N3	0.119	
	Fe−N4	0.075	
6	Fe−S1	0.608	2.768
	Fe−S2	0.657	
	Fe−S3	0.634	
	Fe−N1	0.288	
	Fe−N2	0.292	
	Fe−N3	0.288	

[a] All values were computed from expressions 1−4. Atom labels correspond to those shown in Figure 1.

Equally notably, complexes **1**, **4**, and **6** all have calculated covalencies greater than 2.0|e⁻| suggesting that this is the primary determinant for a low spin ground state in these particular Fe(III) systems. This proposal is consistent with the fact that **2**, **5**, and **3** all have covalencies of less than 2.0|e⁻|. The quartet complexes **2** and **5** still have calculated covalencies of greater than 1.5|e⁻|, however, while the sextet **3** is the least covalent by our measure. In a further interesting observation, we determined that three-center hyperbonding was present for the N1−Fe−S2 interaction but absent for the N2−Fe−S1 interaction in the salen complex **2**, as would be expected from the similar *trans* arrangement of donor and acceptor atoms between these two ligand sets (atom numbering corresponds to that in Figure 1). The DFT-optimized ground spin quartet structure also shows the greatest difference in Fe−N bond lengths of the three spin states explored (Table 3). For example, the Fe−N1 bond length in the experimentally determined structure is somewhat shorter (by 0.051 Å) than the Fe−N2 bond, with approximately equiva-

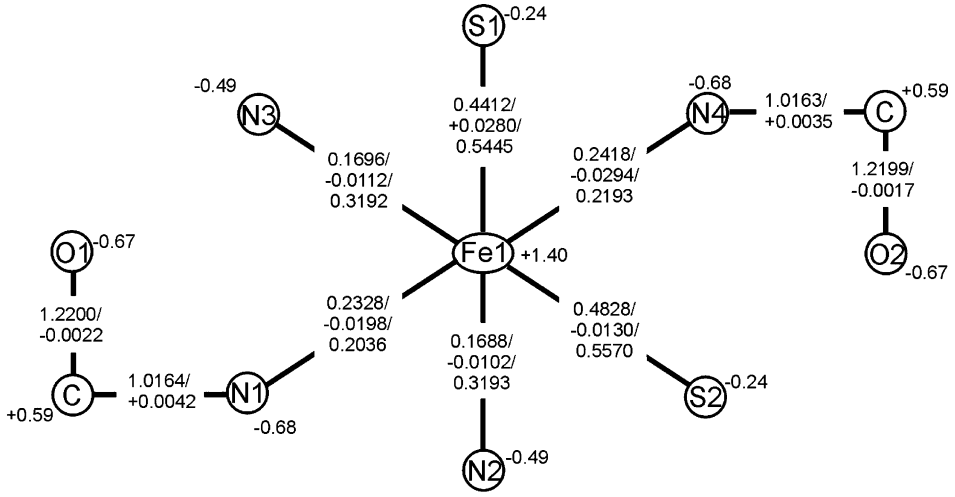

Figure 7. Schematic representation of the metal−ligand bonding in carboxamidato complex **4**. Calculated NPA partial charges are shown adjacent to each atomic center. In each set of numbers associated with a given bond, the NPA/NLMO bond order is given first, and the NPA/NLMO spin polarization is shown second. In cases for which a third value is given, this derived metal−ligand covalency in units of $|e^-|$. Atom labels correspond to those shown in Figure 1.

lent Fe−S bond lengths. This geometric asymmetry is consistent with an analysis of the HOMO − 4 to LUMO + 4 α and β spin orbital energies of this complex (data not shown), which lack any degeneracy associated with square pyramidal coordination. The inequivalent Fe−N bonds in both the experimental and calculated structures suggest that differences in hyperbonding may be critical in rationalization of the spin quartet ground state for complex **2**.

Implications for the Role of Metal Bonding and Ground Spin State in the NHase Active Site. Of the six complexes studied, **4** is the closest structural mimic of the NHase metal center, in that the metal is coordinated by both deprotonated amide and thiolate ligands. As such, a detailed understanding of the bonding in this complex might provide important insight into the precise ligand field determinants of the Fe(III) spin state in the enzyme. The salient features of the bonding around Fe(III) in **4** were therefore characterized (Figure 7). Both deprotonated amides can have two limiting resonance forms: (−N═C(R)−O$^-$), in which charge is localized on the electronegative oxygen atom, and (−N$^-$−C(R)═O), where negative charge is localized on the nitrogen bonded to the positively charged metal ion. The NPA-based partial charges and NPA/NLMO bond orders show the best approximate description of this ligand to be a charge-polarized system, with partial negative charges on both the nitrogen and oxygen atoms, and N−C and C−O bonds that do not exhibit double bond character (Figure 7). Three-center hyperbonding involving the deprotonated nitrogen and the adjacent thiophenyl ring contributes to the Fe−N bonding and delocalizes charge away from the amide nitrogen. Clearly, this is not a feature of the nitrile hydratase active site, where the thiophenyl ring of **4** is replaced by an alkyl α-carbon of the amino acid residue to which the nitrogen belongs. Given that lone pairs on the deprotonated carboxamidato nitrogens of proteins do not have an adjacent potential electron sink other than the peptide carbonyl, the carboxamidato bonding would be expected to be either more charge-polarized, or possibly to exhibit greater C═N double-bond character, than in complex **4**. In either case, deprotonated backbone amide nitrogens should serve as strong donor species to the Fe. These arguments raise the possibility that similar three-center hyperbonding exists in the NHase Fe(III) center, where the metal is ligated by two pairs of *trans* S−Fe−N bonds: αCys-113 and the amide nitrogen of αCys-115, and αCys-115 and the amide nitrogen of αSer-114.[1c] On the other hand, definitive statements about the extent to which such three-center hyperbonding determines the observed low spin Fe(III) configuration are complicated by the fact that both of the cysteinyl sulfur atoms *trans* to the amide ligands are post-translationally oxidized, a structural modification that is required for catalytic activity.[54] Thus, the extent of three-center hyperbonding in the enzyme active site may differ significantly from those seen in complexes **4** given that (i) the oxidized sulfur atoms will be less polarizable than their reduced precursors, and (ii) nearby arginine residues from the NHase β-subunit polarize the S−O bonds, inductively pulling negative charge away from the metal. Resolving the delicate balance between metal−ligand bonding mechanisms and the electronic consequences of post-translational oxidation in NHase will therefore require further theoretical study.

Conclusions

The low spin Fe center of NHase presents a variety of challenges to computational characterization. Although the coordination asymmetry alleviates the need to describe multiple electronic configurations among degenerate one-electron states, spin contamination is still possible if occupied α spin and β spin orbitals do not overlap extensively in the single-determinant Kohn−Sham wave function representation of the density. On the basis of the noninteracting value, the DFT wave functions determined for these open-shell Fe(III) complexes suffer remarkably little from spin contamination, even when the metal is in a low spin state with several available determinants of higher S but identical M_S. These results establish the ability of DFT functionals to optimize the structure of Fe(III) complexes with N/S ligation at various possible spin multiplicities, and to reproduce

correctly the experimentally observed ground state. For almost all of the complexes studied, DFT single point energies computed using the B3LYP functional correctly predict observed ground state spins, the computed energy differences generally lying outside the known errors of the method. Although the BLYP model gives spin state dependent optimized geometries that are consistent with the predictions of ligand field models, this functional seems less reliable than B3LYP for calculating the relative energetics of these Fe(III) complexes, principally because of artificial stabilization of lower spin configurations. Thus, although BLYP is a suitable method for geometry optimization of these Fe(III) complexes, and therefore the NHase metal center, inclusion of orbital-dependent exchange will likely be important in sorting spin energetics at a given geometry.

Natural bond orbital methods also allow a greatly expanded analysis of the Kohn−Sham wave function and facilitate the understanding of bonding features characteristic for a particular spin multiplicity. NPA/NLMO bond orders correlate qualitatively with chemical expectations. For example, Fe−S bonds have more covalent character Fe−N bonds. Using a novel procedure, analysis of the NBO data can be employed to quantitate electron delocalization from ligands onto the metal, and vice-versa. The utility of this method is demonstrated in rationalizing the low spin character of complex **6**, and this approach should be generally applicable to other mononuclear transition metal centers that are amenable to NBO analysis.

Finally, and in contrast to the results of our previous semiempirical calculations,[41] analysis of the NHase model complex **4** shows that the carboxamidato ligands in this complex do not exhibit substantial double bond character in either the carbonyl C−O or the amide C−N bonds. Instead, three-center hyperbonding, as also observed for complexes **1** and **6**, contributes to the metal−ligand covalency in this compound that results in the observed ground state doublet. These studies therefore establish the computational methodology that will be needed to explore the electronic structure and reactivity of the fascinating, and unusual, NHase Fe(III).

Acknowledgment. We thank the National Science Foundation (CHE-0079008) and the National Institutes of Health (DK61193) for support of this work, and acknowledge the National Partnership for Advanced Computational Infrastructure (NPACI) for the provision of supercomputing facilities.

Supporting Information Available: Comparison of the crystallographic and optimized structures of complexes **1**−**6**, details of bond valence sum calculations for complexes **1**−**6** at both their experimental and DFT-optimized geometries, and qualitative diagrams for the d-orbital splitting in idealized square pyramidal and trigonal bipyramidal complexes. This material is available free of charge via the Internet at http://pubs.acs.org.

IC0350032